

STAR FORMATION HISTORY IN THE SOLAR VICINITY

G. BERTELLI

Consiglio Nazionale delle Ricerche, CNR-GNA, Roma, Italy; and Dipartimento di Astronomia, Università di Padova,
vicolo dell'Osservatorio 5, I-35122 Padova, Italy; bertelli@pd.astro.it

AND

E. NASI

Osservatorio Astronomico di Padova, vicolo dell'Osservatorio 5, I-35122 Padova, Italy; nasi@pd.astro.it

Received 1999 August 8; accepted 2000 October 31

ABSTRACT

The star formation history in the solar neighborhood is inferred by comparing a sample of field stars from the *Hipparcos* catalog with synthetic color-magnitude diagrams. We consider separately the main sequence and the red giant region of the H-R diagram. The criteria for our best solutions are based on the χ^2 minimization of star distributions in selected zones of the H-R diagram. Our analysis suggests (1) that the solutions are compatible with a Salpeter initial mass function and with a star formation rate *increasing* in a broad sense from the beginning to the present time, (2) that the deduced volume-mass densities and the corresponding absolute scale of the star formation rate solutions are strongly influenced by the initial mass function slope of low-mass stars (below $0.5 M_{\odot}$), and (3) that the stellar evolutionary models are not completely adequate: in fact the theoretical ratio between the He-burning and MS star numbers is *always a factor of 1.5 greater* than the observational value. This fact could indicate the need for a more efficient overshoot in the evolutionary models or a different mixing theory.

Key words: stars: evolution — stars: formation

1. INTRODUCTION

Determining the past history of star formation from the color-magnitude diagram (CMD) of composite stellar populations in galaxies of different morphological type is one of the main goals of modern astrophysics. For nearby galaxies, in which individual stars are resolved and CMDs are derived, the problem is easier to tackle, as all stars are placed at nearly the same distance. However, in our own galaxy the problem is by far more complicated because there are large fractional differences in the distances of the galactic stars, and only CMDs containing stars of non-homogeneous age, chemical composition, and distance are available. The evaluation of the underlying star formation history requires a few assumptions besides postulating a suitable star formation rate (SFR) when comparing theoretical predictions with observational data. For the sake of illustration, let us consider the case of chemical models designed to interpret the chemical abundances and their spatial gradients in the Galactic disk. In these models the SFR is assumed to be first increasing and then decreasing up to the present time; see for instance model A of Chiappini, Matteucci, & Gratton (1997). But other independent studies suggest that the local SFR has been quite irregular, with periods of enhancement and quiescence showing significant fluctuations (see Rocha-Pinto & Maciel 1996, 1997; Rocha-Pinto et al. 2000 and references therein). Using the chromospheric activity-age distribution of stars in the solar neighborhood, they found a burst of star formation 8 Gyr ago and a lull of activity some 2–3 Gyr ago for the Milky Way. However, the application of their method to the data of Edvardsson et al. (1993) produces an SFR that increases smoothly up to the present.

Recently Hernandez, Valls-Gabaud, & Gilmore (2000) studied the star formation history of the *Hipparcos* solar neighborhood with a maximum likelihood statistical approach combined with variational calculus. They derived an oscillatory component of period ~ 0.5 Gyr, superposed on a small level of constant star formation activity, and the

involved time interval covers the last 3 Gyr. Restriction to this small age range is compelled by the selection criteria (involving limiting magnitude and distance error of the *Hipparcos* sample) required by their method.

The advent of the *Hipparcos* mission set a landmark, as for the first time it was possible to derive the CMD of field stars in the solar vicinity based on accurate distances for each individual object (Perryman et al. 1995). The solar neighborhood sample is very useful for studying our Galaxy's past history, as it is characterized by a large range of ages, distances, and metallicities. In addition to the past star formation history (see Bertelli et al. 1997, 1999), the *Hipparcos* data of field stars have been the subject of several studies aimed at testing stellar evolution theory (see Schröder 1998; Girardi 1999). It is the purpose of this paper to present the results of our investigation for the star formation history of the solar neighborhood on a selected sample of *Hipparcos* data.

2. LOCAL SOLAR NEIGHBORHOOD SAMPLE OF FIELD STARS

In Figure 1a we present the H-R diagram (HRD) for our sample of field stars selected from the *Hipparcos* catalog with the criteria described in § 2.4 below. In Figure 1b we define several regions where we compare the theoretical and observational stellar distributions to test different hypotheses for the SFR under the criteria for χ^2 minimization. The use of characteristic HRD regions has a relevant advantage, since star counts are insensitive to small errors in luminosity and color and to small differences in chemical abundances, provided the sample is adequately populated.

2.1. Completeness

The evaluation of the completeness for our stellar sample is fundamental for any statistical analysis. According to Turon et al. (1992) the *Hipparcos* catalog is essentially complete up to $V \sim 9$ mag, and as reported by Perryman et al. (1995) the limiting magnitude is determined by the sensitivity threshold of its starmapper detectors and depends

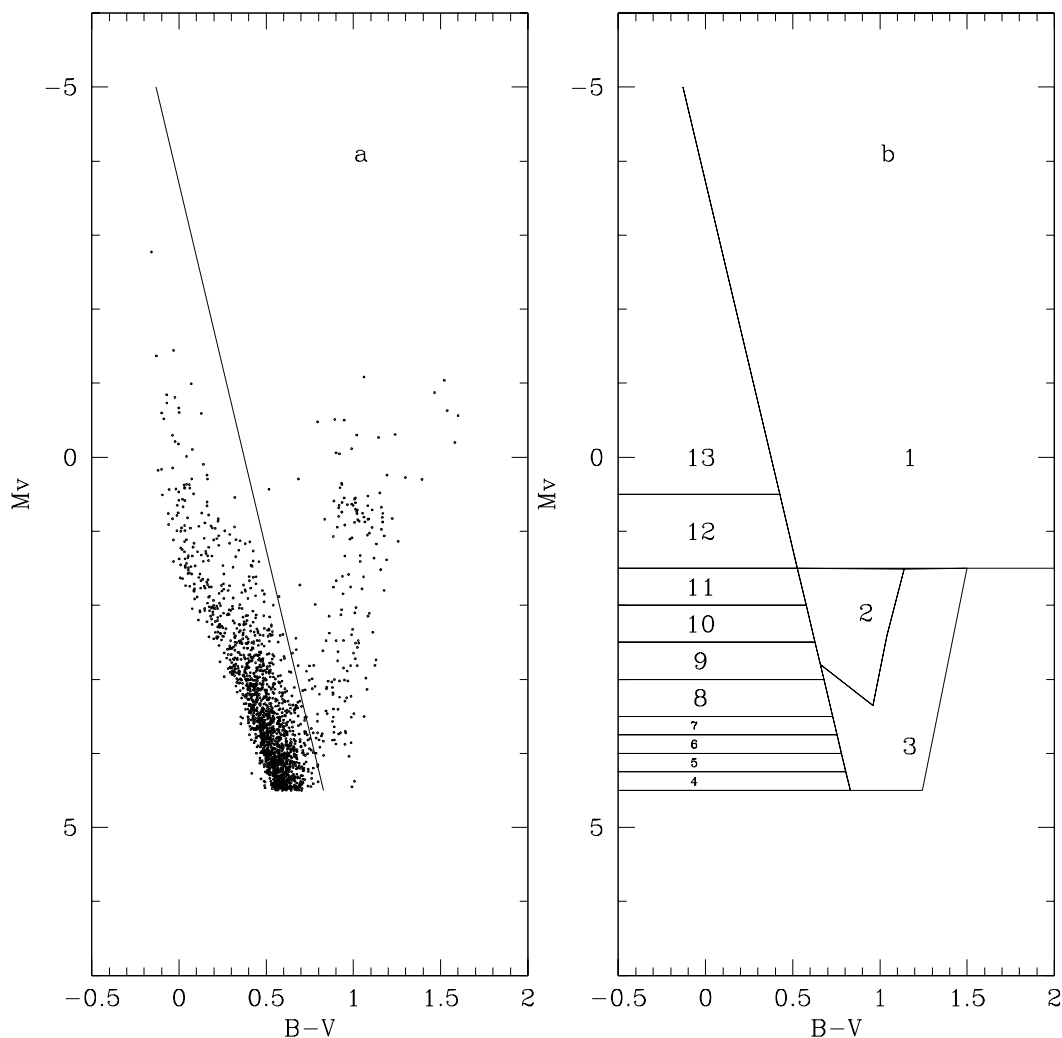


FIG. 1.—(a) Star sample selected from the *Hipparcos* catalog with the criteria described in § 2.4. The transversal line separates the MS from red stars. (b) Star distributions. The HRD zones from 4 to 13 characterize the MS region, while zones 1, 2 and 3 characterize the red region.

on the galactic latitude and the spectral type ($V = 7.9 + 1.1 \sin |b|$ for types earlier than G5 and $V = 7.3 + 1.1 \sin |b|$ for later spectral types).

Schröder (1998) discussed the completeness of the stellar sample based on *Hipparcos* data in his paper on the solar neighborhood HRD as a test of the evolutionary timescales. For an HRD of stars within $d = 100$ pc of the Sun, the sample can be considered to be complete down to $M_V = 4.0$; within $d = 50$ pc, completeness is expected to about $M_V = 5.5$.

As the completeness limit depends on the latitude, we restricted the subsequent counts to HRD regions with M_V brighter than 4.5 to have a reliable completeness down to the low-luminosity end of the considered 50 pc sample.

2.2. Statistical Bias

If stars are selected according to the threshold parallax value ($\pi > \pi_{th}$) and/or if weights are given according to the ratio between its error and the measured parallax (σ_π/π), parallaxes are systematically overestimated and the stars in a volume-limited sample are on average brighter than they appear to be. The corresponding corrections are called Lutz-Kelker (L-K) corrections (Lutz & Kelker 1973). They must be applied to absolute magnitudes and may be evaluated by means of equation (31) in Hanson (1979), where the

parallax distribution is characterized as a power law, $P(\pi) \propto \pi^{-n}$ (for a uniform space distribution, $n = 4$). If the stellar sample under study is wholly or partially magnitude limited, then one expects $n < 4$, which means lower predicted corrections. With fewer stars at smaller parallax, the probability of overestimating an individual parallax measurement is correspondingly reduced (Reid 1997). The resultant L-K corrections strongly depend on the parallax uncertainty, so that the accuracy of *Hipparcos* parallaxes (we select stars with $\pi > 20$ mas and $\sigma_\pi/\pi < 0.1$) limits the L-K bias to magnitude corrections on the order of 0.1 mag at maximum for the case $n = 4$ of uniform space distribution. The safest procedure is to use only stars with good parallaxes ($\leq 10\%$ accuracy), since corrections are negligible for the *Hipparcos* sample considered in our analysis. If stars have a range of luminosities, a magnitude-limited sample would be biased toward luminous objects (Malmquist bias), as the average absolute magnitude is systematically overestimated. The corrections for Malmquist bias have the opposite sign with respect to L-K corrections (they may even compensate for each other).

2.3. Binaries

The high incidence of binaries among field stars (possibly as high as 60%) is a well-established fact (Pont et al. 1998).

When both components have similar luminosities, an unresolved binarity causes an apparent increase of up to 0.75 mag. Because of the sharp dependence of the *Hipparcos* parallax uncertainty on magnitude (Pont et al. 1998), a binary star of a given color has a higher likelihood (than a single star) of being included in a sample selected by σ_π/π limits.

It is necessary to take into account the distribution of binary system mass ratios if we want to introduce binaries in our HRD simulations of the *Hipparcos* sample. There are several papers dealing with these problems. As far as mass ratios are involved, Trimble (1990), Mermilliod et al. (1992), and Mazeh et al. (1992), for example, considered different samples of spectroscopic binaries and found different forms for the distribution function of the mass ratios, probably due more to the selection of binary systems than to the method of analysis. By defining $q = M_2/M_1$, the distribution $N(q)$ is best fitted by a power law near q^{-1} over the range $q = 0.1 - 1.0$, according to Trimble (1990). A similar declining power law has been found for Hyades binaries by Patience et al. (1998), pointing out that there is no mass dependence of the mass ratio distribution. From spectroscopic binaries in the Pleiades Mermilliod et al. (1992) gave a mass ratio distribution reasonably flat for q between 0.4 and 1.0 and no information for the behavior for $q < 0.4$.

There is also a variation of the proportion of binaries with the mass of the primary, as summarized by Kroupa (1993), that ranges from 0.42 for M dwarfs and 0.45 for K dwarfs to 0.53 for G dwarfs. Duquennoy & Mayor (1991), in their paper on multiplicity among solar-type stars in the solar neighborhood, found that only about one-third of the G dwarf primaries may be real single stars. The multiplicity of the massive stars in the Orion Nebula cluster is quite high, on the order of 1.5 companions per primary star on average, after correction for unresolved systems, and about 3 times that among low-mass stars (Preibisch et al. 1999). Binaries were taken into account in our synthetic HRDs, considering the mass ratio distribution and a percentage of double stars varying with mass, as described in § 3.2.

2.4. Selection of the *Hipparcos* Sample

Our sample of stars for the local solar neighborhood taken from the *Hipparcos* catalog has been selected according to the following requirements:

1. All main-sequence or evolved stars within 50 pc of the Sun with a relative parallax accuracy better than 10% are considered (corresponding magnitude completeness limit is down to $M_V = 4.5$). The standard error for $B - V$ is required to be less than 0.025 mag so that the observed data are actually reliable for comparison with theoretical models.

2. From this sample we removed stars belonging to the Hyades cluster according to the list of Perryman et al. (1998), as the cluster may represent a local peculiarity with respect to the average solar vicinity population.

The sample thus derived with these constraints contains 1844 stars, and we consider the corresponding HRD sufficiently populated in the regions of Figure 1a for our analysis of the star formation history.

Double and multiple systems were taken into account according to the information given in the catalog (ESA 1997). There are resolved systems with or without separate entries for the components, but most of the systems are

unresolved. Dealing with all the many cases of multiplicity is very complicated; thus we will take into account binarity with a few simplifications, being aware that there are also some selection effects (like undetected and/or undetectable binaries for observational limits) that we are not able to take into account. As a starting point we identified the number of binary systems in each of the different HRD regions defined in Figure 1b. Then we used this percentage of binaries when computing the synthetic HRD.

3. COMPARING THE OBSERVATIONS WITH THEORETICAL MODELS

3.1. Preliminary Technique and Results

Comparing the color-magnitude diagram (CMD) of a stellar population with theoretical isochrones or synthetic HRDs is a technique to derive information on the age, chemical composition, SFR, and initial mass function (IMF) of the considered population. By simply superposing a few selected isochrones with solar chemical composition on the observed HRD of the *Hipparcos* sample, we can derive some preliminary insights for the solar vicinity:

1. Star formation began about 10 Gyr ago: $T_i = 10$ Gyr. This is determined from the red envelope of subgiant and giant branch stars. Jimenez, Flynn, & Kotoneva (1998) suggested a minimum value on the order of 8 Gyr for the galactic disk, derived essentially by fitting isochrones to the subgiant region of the *Hipparcos* sample. Combining kinematic information with the local color-magnitude diagram, Binney, Dehnen, & Bertelli (2000) deduced a solar neighborhood age of 11.2 ± 0.75 Gyr. Our value of 10 Gyr is between these two age determinations and is also supported by the results of the age determination of open clusters by Carraro, Girardi, & Chiosi (1999), who suggest an age of about 9–10 Gyr for the Galactic disk. Because of uncertainties in stellar evolutionary models we cannot associate an error with our age estimate. In § 7.3 we report on the effects of changing the initial age, T_i .

2. The star formation stopped around 100 million years ago: $T_f = 0.1$ Gyr.

3. The solar neighborhood cannot be described by a single chemical composition. It is evident from the width of the main-sequence band and also from the color extension of the horizontal-branch clump that there is an extended range of chemical composition of the observed stars. From the comparison between isochrones with different metal content (Bertelli et al. 1994) and the observations, we conclude that the majority of the stars must have a chemical composition in the range $0.008 \leq Z \leq 0.03$. This choice of the chemical composition is supported by the results of extensive spectroscopic observations of selected nearby F and G stars by Edvardsson et al. (1993).

3.2. Synthetic HRD Technique

The analysis of the CMD of our selected sample relies on the synthetic HRD technique (ZVAR; Bertelli et al. 1992; Vallenari et al. 1996a, 1996b; Aparicio, Gallart, & Bertelli 1997a, 1997b; Gallart et al. 1996, 1999). It requires the following information:

The shape of the star formation rate.—We will use two very simple hypotheses shown in Figures 2a–2b, where the verti-

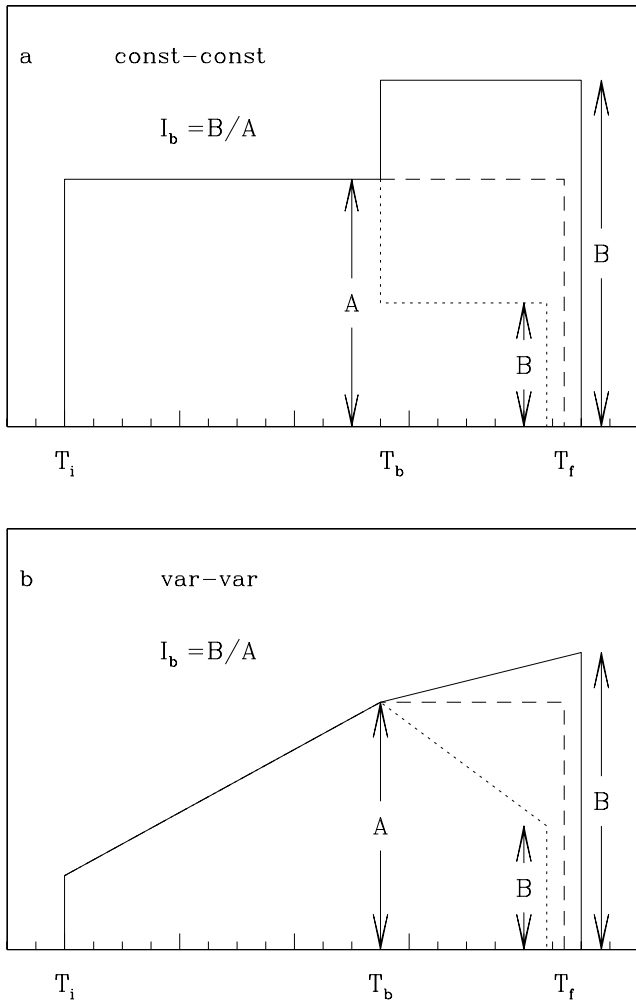


FIG. 2.—(a) Shape of the SFR, as described in § 3.2 for the const-const model, where T_b is the time of the rate change and I_b is the ratio of the SFR at the final time, T_f , to its value at T_b . (b) Same as (a), but for the var-var model. In both panels the final time, T_f , is the same for all the shapes, but it is plotted separately for clarity.

cal scale is arbitrary. The absolute values of the SFR scale will be fixed from the total amount of mass converted in stars (in solar masses and computed for each synthetic model). The normalization imposed on the models requires the same number of MS stars as in the *Hipparcos* sample (1658 stars more luminous than $M_V = 4.5$). In § 8 we derive the local mass density. In the following we keep the initial time T_i (at which star formation began) and the final time T_f (at which star formation ceased) fixed at the values suggested by the preliminary results (§ 3.1). There are two hypotheses for the star formation rate. (a) The const-const model is a combination of two steady periods with a discontinuity at time T_b , in which T_b is allowed to vary between T_i and T_f . The ratio between the SFR at the age T_f and that at T_b is represented by the parameter I_b ($= B/A$) and can also vary (Fig. 2a). The model for which the SFR rate is constant over the entire time interval is a particular case ($I_b = 1$). (b) The var-var model represents the case in which the SFR increases by a factor of 3 during the first time interval, from T_i to T_b , and then the change of the SFR slope is characterized by the choice of the parameter I_b (Fig. 2b). We considered possible solutions, varying the parameters T_b and I_b , in our analysis (§§ 5 and 6). We also checked the influence of

different values of T_i (§ 7.3). It is evident that the var-var model can describe many different SFR shapes, from the Milky Way chemical evolution model by Chiappini et al. (1997), where the SFR first increases and then decreases to the present age, to cases in which the rate is continuously increasing or decreasing. Our method can recognize broad trends in the star formation rate during this long time interval (10 Gyr ago), but it is not useful to trace fluctuations of short duration.

The initial mass function.—The IMF is defined by

$$dN \propto M^{-x} dM, \quad (1)$$

for which we initially assume the classical Salpeter law with $x = 2.35$. We also considered other power-law values (§ 7.1). *The relative lifetime spent by stars in each elemental area of the HRD.*—This is derived by interpolation on an extended set of masses and chemical compositions from the Padua library of stellar models (see references of the whole set of models in Bertelli et al. 1994).

Chemical composition.—Edvardsson et al. (1993) and Ng & Bertelli (1998) did not find an age-metallicity relation for field stars but a large scatter in metallicity ($0.008 < Z < 0.03$). Then in each simulation the metallicity is stochastically varied from star to star within this range.

Binaries.—In the simulations we adopted the percentage of binaries per magnitude interval as obtained from the *Hipparcos* sample, according to the identification and/or flags in the catalog (decreasing from 0.70 for the more massive primaries to about 0.27 at the faint limit, at $M_V = 4.5$). As far as the mass ratio q of the system is involved, we took into account two different observational results; first, according to Trimble (1990) the distribution $N(q)$ is described by a power law (q^{-1}) over the range $q = 0.1-1.0$; second, according to Mermilliod et al. (1992) there is a flat distribution between 0.4 and 1. Of course this second distribution, giving no information about the behavior for $q < 0.4$, suffers from the limit of neglecting the low mass-ratio companions, whose effective number nobody knows. On the other hand, if the primary is rather more massive than the companion, its magnitude and color are almost the same as those of a corresponding single star.

4. CRITERIA FOR BEST SOLUTIONS

To obtain the best solutions for our models we separately compared the data for the main-sequence stars (MS) and evolved stars (red), which are identified by the separation line shown in the color-magnitude diagram of Figure 1a. The luminosity interval spanned by the main-sequence stars is divided into 10 bins (zones 4–13 in Fig. 1b). For both particular shapes of the SFR (const-const and var-var) many combinations of T_b , I_b , and x have been examined. For every model, 20 simulations of the CMD have been generated using the observed number of MS stars as the normalization parameter. We assume that the SFR (for given IMF) of the model reproduces the features of the observed sample with a reasonable agreement when the following two criteria are satisfied:

MSa.—The value of

$$\chi_{\text{ms}}^2 = \sum_{i=1}^n \left[\frac{(N_{\text{obs}} - \langle N_{\text{mod}} \rangle)^2}{\langle N_{\text{mod}} \rangle} \right]_i \quad (2)$$

must be minimized. N_{obs} and $\langle N \rangle_{\text{mod}}$ are the number of stars in the i th MS zone of the HRD, from the observations and from the model (averaging over the 20 simulations), respectively, and n is the total number of MS zones ($n = 10$). The probability distribution function for χ_{MS}^2 is tabulated (Bevington 1969). In our case there are seven degrees of freedom. If we require that the probability of the χ_{MS}^2 be greater than $P = 0.1$, we deduce that the acceptable minima must be below a critical value of 12. For greater values of χ_{MS}^2 the probability of obtaining such a large value of χ_{MS}^2 with the correct SFR is smaller than 0.1, indicating that the SFR actually used may not be appropriate. We will test this method with numerical simulations presented in the next section.

MSb.—For the second MS criteria the Kolmogorov-Smirnov test (K-S) is used. It can discard with high probability models for which the agreement between the observed and simulated CMD must be excluded. We have discarded models for which the probability P coming from this test is lower than $P = 0.1$ (see Press et al. 1986 for more information on the K-S test). The 20 simulations were considered all together for the K-S test.

The red region has been divided in three zones. Zone 1 in Figure 1b contains all red stars brighter than $M_v = 1.5$. Since the majority of these stars are in the central He-burning phase we refer to them using the subscript He. The other two “red” zones (zone 2 and zone 3 in Fig. 1b) have been selected in such a way that the ratio between the number of stars in zone 2 and that in zone 3 (R_{red}) indicates the spread of the evolved stars below the luminosity limit $M_V = 1.5$. The majority of the simulations shows that these stars are concentrated in a narrow band inside zone 3 and that there are no stars in zone 2 ($R_{\text{red}} = 0$). A further significant indicator of the star distribution is the ratio $R_{\text{He/MS}}$ between the number of stars in the He-burning phase, N_{He} , and that in the main-sequence phase, N_{MS} . This ratio is *not* very sensitive to the details of the SFR, while it depends on the IMF parameter x and on the stellar structure (for example, on the overshoot parameter λ). To identify the models that give a satisfactory representation of the red part of the HRD we consider the following criteria:

Ra.—The quantity χ_{red}^2 (similar to χ_{MS}^2 but for the red zones 1, 2, and 3) must be minimized. In this case, because of the small number of zones, there are zero degrees of freedom, and the statistics of the distribution of χ_{red}^2 is not known; we have done numerical experiments suggesting that the minimum must be below the value $\chi_{\text{red}}^2 = 5$.

Rb.—The observed R_{red} must be within $\pm 1 \sigma$ of the mean value obtained by the 20 simulations, where σ is the standard deviation.

Rc.—The observed ratio $R_{\text{He/MS}}$ must be within $\pm 1 \sigma$ of the mean value obtained by computations.

5. TEST OF THE METHOD

In this section we test the reliability of the criteria adopted in evaluating the results. We proceed in a similar way to that in Gallart et al. (1999). We compute a stellar population with a given star formation rate and known input parameters (i.e., $T_i = 10$ Gyr, $T_f = 0.1$ Gyr, metal content Z chosen stochastically in the range 0.008–0.03, IMF parameter $x = 2.35$, binarity percentage as in *Hipparcos* data, and the distribution of the mass ratio as in Trimble 1990). We used the same number of stars as the *Hipparcos*

sample since we considered this simulated sample as an observed one. The particular SFR adopted for this test is *constant* over the entire time interval.

For a fixed value of I_b (six cases are investigated, namely, $I_b = 0.2, 0.6, 1.0, 1.5, 2.0,$ and 2.5), the corresponding values of χ_{MS}^2 and χ_{red}^2 are computed for T_b values varying from T_i to T_f and spaced by 1 Gyr. We expect to single out the values of T_b and I_b corresponding to a minimum of the χ^2 functions and require that the previously defined criteria for the main sequence and the red region be satisfied.

We begin with the const-const case (see Fig. 2a) for the SFR. In Fig. 3a the results for the function χ_{MS}^2 are presented. The continuous lines with increasing thickness correspond to increasing values of I_b (0.2, 0.6, and 1.0). The dotted line, dot-short-dashed line, and dot-long-dashed line refer to the values $I_b = 1.5, 2.0,$ and 2.5 , respectively. The line corresponding to $I_b = 1.0$, which means a constant SFR (independent of T_b) fluctuates between 6 and 10 below the critical value $\chi_{\text{MSC}}^2 = 12$ and around a horizontal mean line; this mean line represents a lower value with respect to all other cases considered for I_b . For the specific case $I_b = 1$ all models satisfy the K-S test. In the figure all models that satisfy the K-S test are indicated with a black square. The

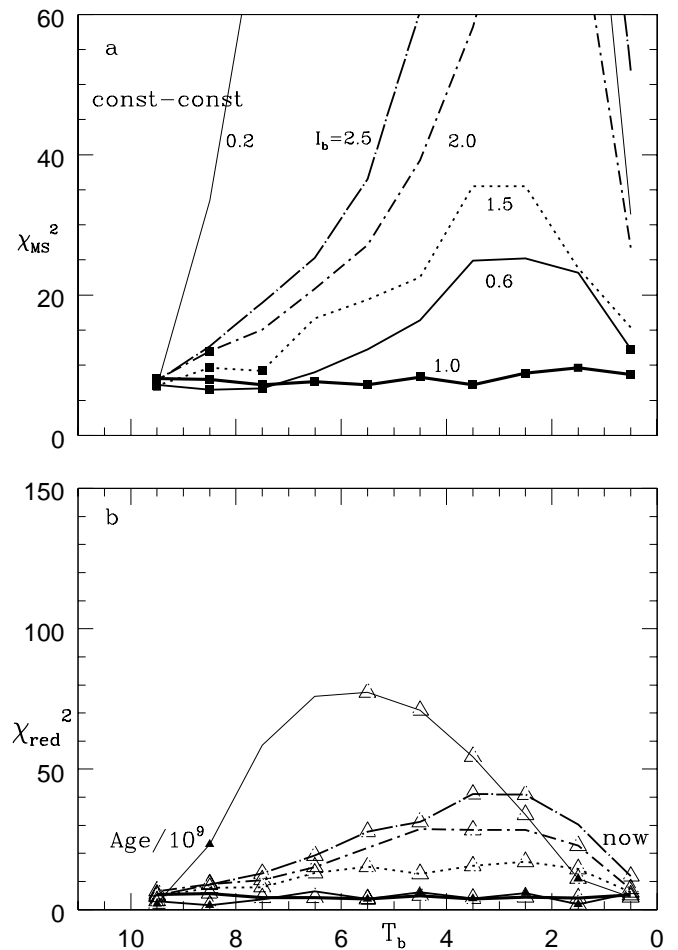


FIG. 3.—(a) Values of χ_{MS}^2 computed for the SFR const-const model and with IMF $x = 2.35$ to test the simulated sample (produced with constant SFR and $x = 2.35$). T_b varies between T_i and T_f , spaced by 1 Gyr. Each line corresponds to a different value of I_b . Squares indicate models whose probability P from the K-S test is greater than 0.1. (b) Same as (a) but for χ_{red}^2 . Solid triangles indicate that condition Rb is satisfied; open triangles correspond to models that satisfy condition Rc.

main result is that a constant SFR was recovered. However there is some degeneracy. In fact, when T_b approaches T_i , several other curves (the curves $I_b = 0.6$ and 1.5) reach values of χ_{MS}^2 in the range 6–10, and this method is unable to disentangle these solutions. In any case the result of the analysis with a const-const model is consistent with an SFR constant during the majority of the lifetime of the system (at least during the last 8 Gyr).

The results from the red part of the HRD support our previous analysis. In fact, as shown in Fig 3b, there are two curves that fluctuate around a straight line below the value $\chi_{\text{red}}^2 = 5$, the curve $I_b = 1$ (constant SFR) and the curve $I_b = 0.6$, so that condition Ra is satisfied. They also satisfy condition Rb (models indicated with a solid triangle) and condition Rc (models indicated with an open triangle). We point out that for almost all the values of I_b and T_b condition Rc relative to the ratio $R_{\text{He/MS}}$ is satisfied (it is within $\pm 1 \sigma$ of the “observed” value). This means that this ratio is insensitive to the particular shape of the SFR. The analysis for the var-var model confirms a constant SFR at least during the last 8 Gyr.

The fact that different solutions give the same information, that is, a constant SFR during the majority of the system lifetime, except for some indeterminacy at the beginning, should clearly indicate that this method is not capable of determining the detailed shape of the SFR but simply the trend over the total life of the system.

We repeated the same analysis for two values of the IMF slope ($x = 1.35$ and $x = 3.35$ (recall that the simulated sample was derived with $x = 2.35$). In both cases the analysis did not yield acceptable solutions.

6. APPLICATION TO THE *Hipparcos* SAMPLE

We now present our results using the *Hipparcos* sample in which we adopted the input parameters already discussed at the beginning of § 5.

6.1. Const-Const Models

In Fig. 4a we present, as a function of T_b and I_b , the trend of χ_{MS}^2 for the main-sequence stars. The squares in the figure mark those models whose probability P from the K-S test is higher than 0.1. From the figure we notice that the three curves characterized by $I_b > 1$ (curves for $I_b = 1.5, 2.0$, and 2.5) reach minimum values of χ_{MS}^2 below the critical value, 12. The corresponding solutions are, respectively, 2.5 Gyr for $I_b = 1.5$, 4.5 Gyr for $I_b = 2.0$, and finally 5.5 Gyr for $I_b = 2.5$. For the models around the minima also the K-S test yields acceptable results.

In Fig. 4b the curves χ_{red}^2 (for the red part of the HRD) corresponding to the same models of Fig. 4a are drawn. There is a broad minimum for $I_b = 2.0$ and 2.5, with low values of χ_{red}^2 with respect to all other curves, even though this minimum is on the order of 25 (5 times the expected value). Consequently condition Ra is not satisfied; the age range is slightly shifted to younger values with respect to those obtained for the main sequence. Furthermore, no models satisfy conditions Rb and Rc in correspondence of the χ_{red}^2 minima.

6.2. Var-Var Models

In Fig. 5a, χ_{MS}^2 versus T_b is shown. There are several models that could fit the observed distribution of the MS stars. In the range 6.5–9.5 Gyr the curves $I_b > 1$ attain a minimum or fluctuate around low values of χ_{MS}^2 (below the

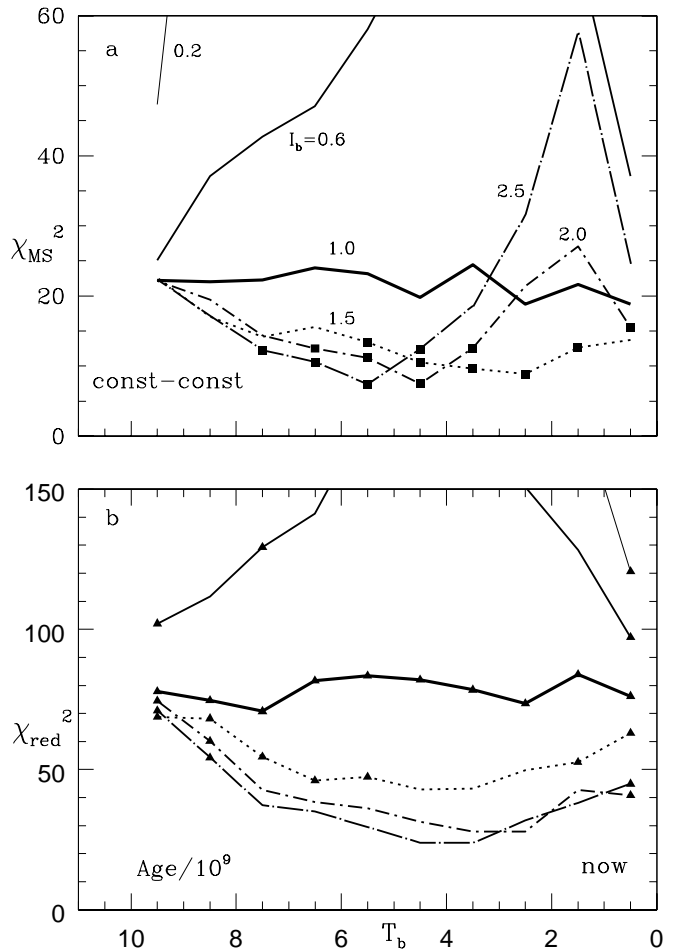


FIG. 4.—Analysis of the *Hipparcos* sample with SFR const-const model and IMF $x = 2.35$. (a) χ_{MS}^2 for main-sequence stars distribution. (b) χ_{red}^2 for red stars. Symbols are the same as in Fig. 3a–3b.

critical value, 12, as shown in the figure) where the requested condition on the K-S test is also satisfied. In the range 1.5–3.5 Gyr, solutions are possible also for the case $I_b = 1$; this means that the SFR was increasing by a factor of 3 from the beginning until 1.5–3.5 Gyr ago and then remained constant to the present. It could seem that the result of the analysis is not very coherent, but all the models suggest an increasing SFR on average from the beginning up to now. For the red region we meet the same difficulties already described in the previous case. In particular all models that could be considered good solutions on the basis of the main-sequence analysis yield χ_{red}^2 values (Fig. 5b) that are 4–5 times higher than the critical value obtained in the test of § 5 and in consequence fail to meet the significant condition Rc. In fact the ratio $R_{\text{He/MS}}$ fluctuates around a value that is about 1.5 times the observed one for all the models. With the IMF parameter $x = 2.35$ and the particular shapes of the SFR adopted, we could not find solutions satisfying the required conditions for the MS and the red region at the same time.

It is well known that there are significant uncertainties in stellar models due to the treatment of convective mixing and the consequent derivation of convective zones border (overshoot problem). These uncertainties affect the H- and He-burning lifetimes and their ratio, as well as the expected number of stars in blue or red regions of the HRD. Our models (synthetic HRD) are normalized to the observed

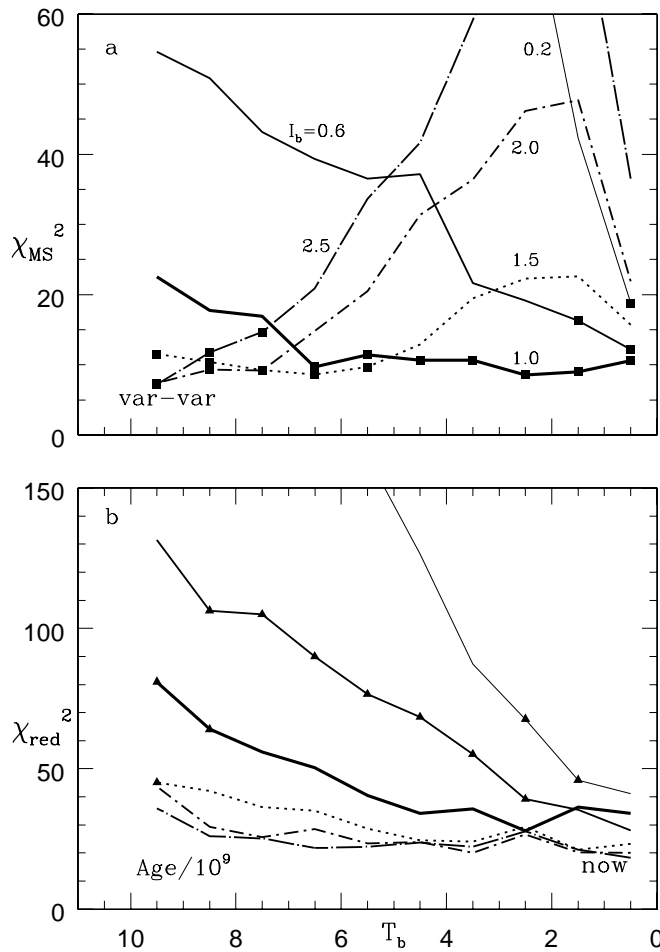


FIG. 5.—Analysis of the *Hipparcos* sample with SFR var-var model and IMF $x = 2.35$. Symbols are the same as in Fig. 3a–3b.

number of main-sequence stars, so that if the adopted overshoot treatment is not fully correct the major consequences will appear in the red part of the HRD. We decide to give up the constraints Rb and Rc and to keep the condition that χ_{red}^2 must show the lowest values with respect to all considered models, assuming that the Salpeter IMF is a reasonable choice and that the overshoot parameter λ used in our stellar models is not well calibrated. With these relaxed conditions for the red region (χ_{red}^2 minimum on the order of 20–30), the best solutions for the SFR parameters I_b and T_b are presented in Table 1.

7. EFFECTS OF CHANGING THE INPUT PARAMETERS

7.1. IMF Parameter x

We explore other values for the IMF parameter to look for its influence on the results. The cases $x = 1.35$ and $x = 3.35$ have been considered.

TABLE 1
GLOBAL SOLUTIONS (MS AND RED
REGIONS) FOR $x = 2.35$

Model	I_b	T_b
A, Const-Const	2.0	4.5
B, Const-Const	2.5	5.5
C, Var-Var	1.0	2.5
D, Var-Var	2.0	7.5–8.5

7.1.1. Case for $x = 1.35$

The const-const model presents a reliable solution for the MS region, given by a deep minimum at $T_b = 1.5$ Gyr, with the parameter I_b equal to 0.6. The red counterpart of the MS solution is completely unsatisfactory as χ_{red}^2 is greater than 140 and the ratio $R_{\text{He/MS}}$ is about 2 times greater than the observed value (its value fluctuates around 0.093 for all the models and combinations of T_b and I_b). We show Figure 6a–6b for the const-const model, which can be compared with $x = 2.35$ in Figure 4a.

7.1.2. Case for $x = 3.35$

Figures 7a–7b show the curves χ_{MS}^2 and χ_{red}^2 as a function of T_b for the var-var model. χ_{MS}^2 reaches a minimum higher than the critical value for $I_b = 2.5$ at $T_b = 1.5$ Gyr. The corresponding χ_{red}^2 reaches a low value (on the order of 5), representing an acceptable solution. The most interesting result is that the ratio $R_{\text{He/MS}}$ remains around 0.05, very near to the observed value (0.047) for all the possible choices of the star formation rate, as indicated by the open triangles in Figure 7b.

Even though for this model we have the best solution for the red region (in fact, all conditions Ra, Rb, and Rc are satisfied), in accordance with the discussion in § 6 we decide to give more credit to the results from the MS region that are at the limit of acceptance for this value of the IMF slope.

We can conclude that in our opinion the best-founded results are those obtained for the $x = 2.35$ case.

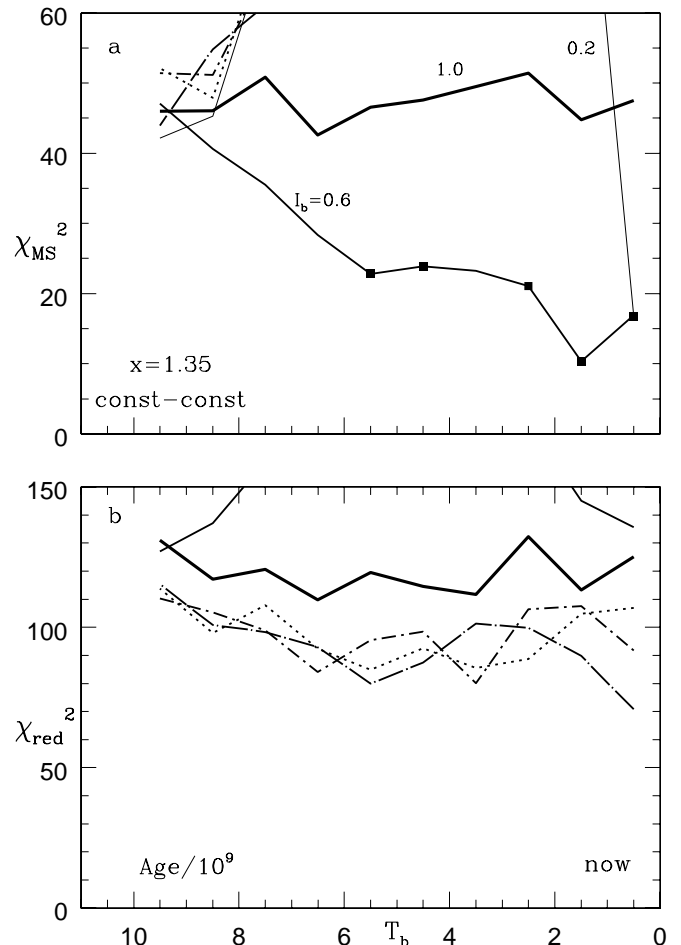


FIG. 6.—Analysis of the *Hipparcos* sample with SFR const-const model and IMF $x = 1.35$. Symbols are the same as in Fig. 3a–3b.

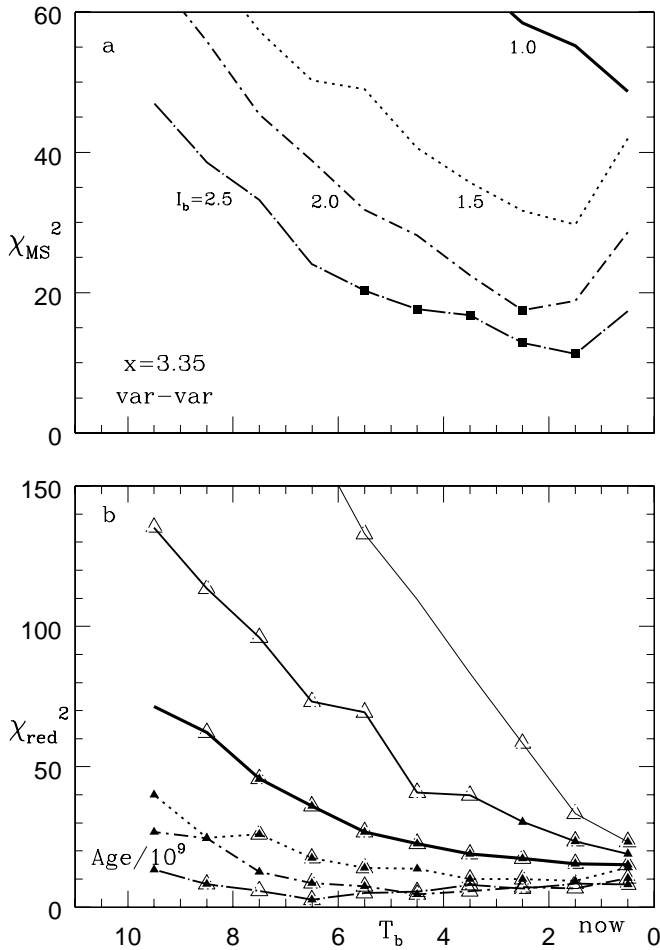


FIG. 7.—Analysis of the *Hipparcos* sample with SFR var-var model and IMF $x = 3.35$. Symbols are the same as in Fig. 3a–3b.

7.1.3. Degeneracy between IMF and SFR

The degeneracy between the SFR and the IMF is evident from the previous discussion about the cases $x = 1.35$ and $x = 3.35$. As far as the MS is concerned, we find that a flat IMF ($x = 1.35$) favors a decreasing SFR, as indicated by the solution with $I_b = 0.6$ for the const-const model, while a steep IMF ($x = 3.35$) requires an increasing SFR characterized by $I_b = 2.5$ in the var-var model. The ratio $R_{\text{He/MS}}$ changes by approximately a factor of 2 from $x = 1.35$ to $x = 3.35$. As soon as the uncertainties on stellar evolutionary lifetimes are removed, the information from the HRD red region could partly eliminate this degeneracy.

7.2. Binary Percentages and Mass Ratio Distributions

We analyzed the effects of changing the percentage of binaries on the models. We considered two cases, setting the percentage of binaries at 75% or 50% of the total number of stars independently of the visual magnitude. The results are not very much influenced by these changes. Also the effect of the shape of the distribution of the mass ratio has been considered; in place of Trimble’s (1990) distribution (as used in all previous computations), a flat distribution between 0.4 and 1.0 (according to Mermilliod et al. 1992) has been considered, and also in this case the effects on the results are negligible. The effects become considerable only when the mass ratio of the binary system is near unity, producing a flatter SFR than that of the previous results.

7.3. Initial Age T_i

We considered $T_i = 8$ Gyr and $T_i = 12$ Gyr. The adoption of a rejuvenated initial age ($T_i = 8$ Gyr) has the effect of flattening the SFR. In fact we find a constant SFR as an acceptable solution by analyzing the sample with the const-const model. An older value of the initial age ($T_i = 12$ Gyr) does not modify the general conclusions presented in § 6 for the const-const and var-var models: a star formation rate increasing (in a broad sense) from the beginning up to now.

8. LOCAL STAR FORMATION RATE AND MASS DENSITY

The *Hipparcos* data allow the assessment of the amount of matter in the local Galactic disk (Holmberg & Flynn 2000), first, because of the information on the kinematics and the vertical density distribution of stars and, second, because of the measurement of the local luminosity function. From a volume-complete sample of A and F stars Holmberg & Flynn (2000) derived an estimate of $0.095 M_\odot \text{pc}^{-3}$ in visible disk matter. Other determinations of the local mass density have been made by Cr ez e et al. (1998), who estimated the total amount of gravitating matter at $0.076 \pm 0.015 M_\odot \text{pc}^{-3}$, and by Pham (1997), who derived a local dynamical density $\rho_0 = 0.11 \pm 0.01 M_\odot \text{pc}^{-3}$.

We must point out that all our previous discussions involved only the more luminous part of the HRD ($M_V \leq 4.5$) and all tests with different values of the IMF slope used only stars with masses greater than about $0.9 M_\odot$. The absolute scale of the SFR is determined by the total mass converted into stars, computed by imposing the same number of MS stars as in the *Hipparcos* sample and extending the HRD simulations down to the low limit of the main sequence ($0.1 M_\odot$) for the given IMF.

Two possible choices for the power-law IMF parameter have been considered: (a) $x = 2.35$ (Salpeter) in equation (1) over all the mass range and (b) two different IMF slopes depending on the mass range: $x = 1.3$ for masses between 0.1 and $0.5 M_\odot$ (from Kroupa et al. 1993) and the Salpeter slope for masses greater than $0.5 M_\odot$. This second hypothesis is indicated with TS IMF, for “Two Slope IMF”. In Figure 8 we show the SFR per unit volume and time computed for the solutions in Table 1, taking into account low-mass stars with the TS IMF hypothesis. In Table 2 we present the volume density derived for the two IMF cases considered for the same Table 1 models. The stochastic fluctuations of the total mass per unit volume due to the normalization to the small number of observed stars determine the standard deviations for the volume density, which is at maximum 6% of the values reported in Table 2.

The most interesting points are the following:

1. Given the low-mass IMF, the derived volume densities corresponding to different SFR models are in a very narrow range, confirming a common characteristic in all solutions:

TABLE 2
VOLUME MASS DENSITY IN $M_\odot \text{pc}^{-3}$ IN THE SOLAR VICINITY

SFR Model	Salpeter IMF	TS IMF
A	0.10	0.071
B	0.098	0.072
C	0.10	0.074
D	0.099	0.072

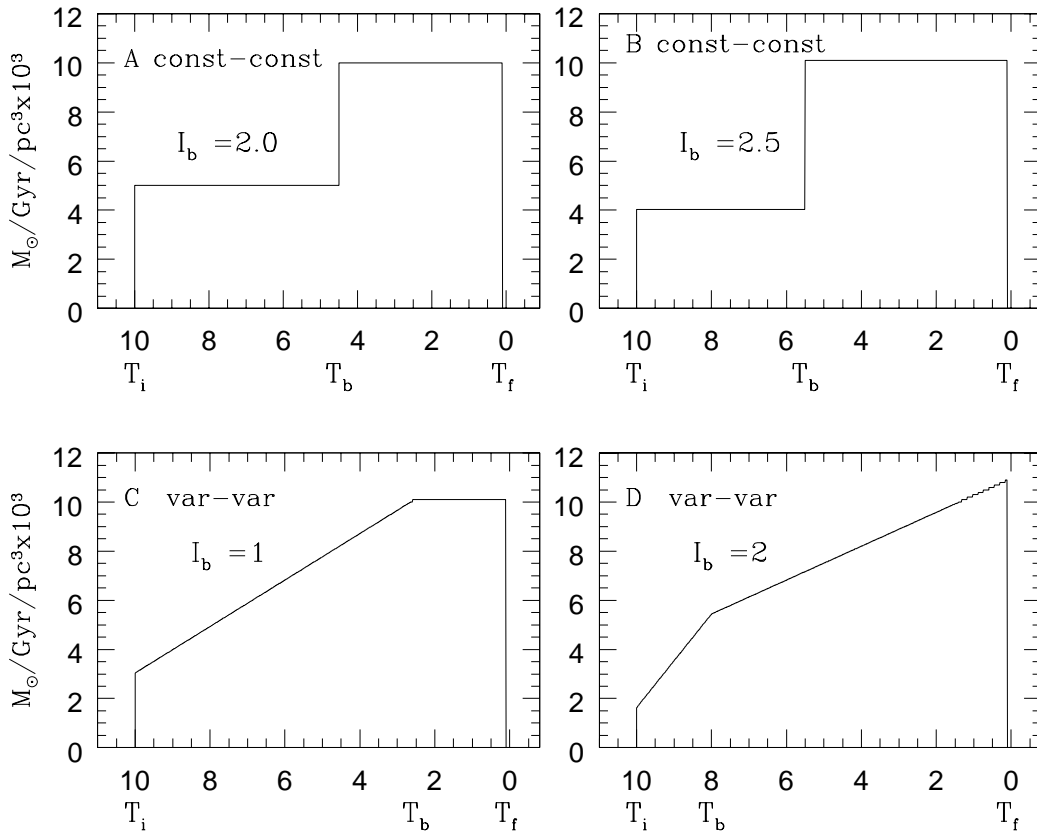


FIG. 8.—Star formation rate per unit volume in $M_{\odot} \text{ Gyr}^{-1} \text{ pc}^{-3}$ relative to the acceptable solutions in Table 1. The SFRs were computed with initial mass function including the low-mass stars for the case TS IMF described in § 8. Ages are expressed in gigayears.

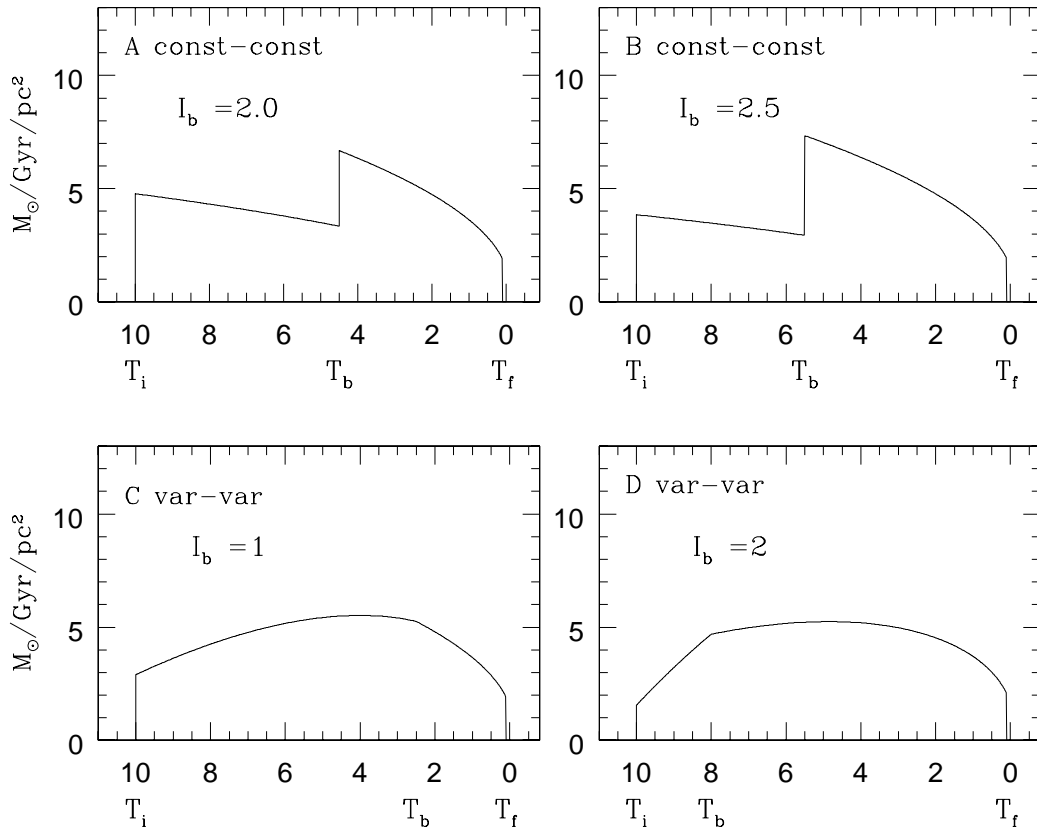


FIG. 9.—Star formation rates per unit surface area in $M_{\odot} \text{ Gyr}^{-1} \text{ pc}^{-2}$ derived from the models in Fig. 8, accounting for the fraction of stars of age t over the disk thickness, relative to those inside a sphere of given radius. Ages are expressed in gigayears.

TABLE 3
SURFACE MASS DENSITY IN $M_{\odot} \text{ pc}^{-2}$ IN
THE SOLAR VICINITY

Model	Salpeter IMF	TS IMF
A	62	44
B	59	44
C	62	45
D	60	44

the star formation rate increases, in a broad sense, from the beginning to the present time. The term “broad sense” is justified by the results in Figure 8, as the SFR at the beginning was in all cases smaller by a factor 2–5 than the present one.

2. The differences between the volume density derived with a Salpeter law ($\sim 0.10 M_{\odot} \text{ pc}^{-3}$) and that with TS IMF ($\sim 0.07 M_{\odot} \text{ pc}^{-3}$) are significant and clearly due to the different IMF slope in the mass range from 0.1 to $0.5 M_{\odot}$. Because of the standard deviations in the volume density, there is an error of the same magnitude (6%) for the SFR in Figure 8. This uncertainty is negligible with respect to the relative difference in the SFR value (on the order of 40%) corresponding to the two different IMF hypotheses.

3. Estimates of the local mass density of the ISM yield $0.04 M_{\odot} \text{ pc}^{-3}$ (Fuchs, Jahreiss, & Flynn 1998; Cr ez e et al. 1998; Holmberg & Flynn 2000 and references therein), but errors by a factor of 2 or more are not excluded. Our lower value of the stellar mass density ($\sim 0.07 M_{\odot} \text{ pc}^{-3}$) is obtained for the TS IMF case. If $\sim 0.1 M_{\odot} \text{ pc}^{-3}$ is the observed value of the dynamical mass density and $0.01 M_{\odot} \text{ pc}^{-3}$ the local mass density of brown dwarfs (Fuchs et al. 1998), filling the gap between the dynamical mass determinations and the mass density of stars (luminous and brown) requires a drastic reduction of the ISM mass density on the order of 50%. In the case of the dynamical mass obtained by Cr ez e et al. (1998), the reduction imposed on the ISM would be even more significant.

4. The high values obtained for the volume density with the Salpeter hypothesis for the entire mass range favors the TS IMF choice for the low-mass range ($0.5\text{--}0.1 M_{\odot}$). The discussion in point 3 also supports the TS IMF results.

As the vertical velocity dispersion relative to the galactic plane depends on the age of the considered population, each population of given age is characterized by different scale heights that increase with age. Following Hernandez et al. (2000) and based on the results of Kuijken & Gilmore (1989a, 1989b), it is possible to derive the fraction of the total number of stars of age t over the disk thickness relative to those inside a sphere of given radius. This procedure takes into account the details of the vertical disk force law and the variations of velocity dispersion with age, which require a larger correction factor as a function of the age.

Knowing that fraction as a function of time from the models in Figure 8, it is possible to derive the star formation rate expressed in $M_{\odot} \text{ Gyr}^{-1} \text{ pc}^{-2}$. The results are shown in Figure 9. The present SFR in the solar neighborhood is on the order of 2 for all the TS IMF models. The observational estimates are between 2 and $10 M_{\odot} \text{ Gyr}^{-1} \text{ pc}^{-2}$; see G usten & Mezger (1982). By integrating over time we obtain the total surface mass density in $M_{\odot} \text{ pc}^{-2}$. The results are presented in Table 3 for the two IMFs considered. For the TS IMF case the total density of the stellar

component is in the range $44\text{--}45 M_{\odot} \text{ pc}^{-2}$, in agreement with recent evaluations ($50 M_{\odot} \text{ pc}^{-2}$, Kuijken & Gilmore 1989a; $48 M_{\odot} \text{ pc}^{-2}$, Kuijken & Gilmore 1991; $49 M_{\odot} \text{ pc}^{-2}$, Flynn & Fuchs 1994; $45 M_{\odot} \text{ pc}^{-2}$, Englmaier & Gerhard 1999; $48 M_{\odot} \text{ pc}^{-2}$, Holmberg & Flynn 2000).

9. DISCUSSION AND CONCLUSIONS

We determined the star formation rate for the solar neighborhood using the *Hipparcos* selected sample and our theoretical stellar models. Taking into account different SFRs and IMF slopes, we analyzed the main-sequence region separately from the red region of the HRD. The main results are the following:

1. All the accepted solutions, shown in Table 1, support a star formation rate that was increasing, in a broad sense, from the beginning (10 Gyr ago) up to the present time. The range of stellar masses involved in the *Hipparcos* sample (for which $M_V \leq 4.5$, corresponding to $M \geq 0.9\text{--}1.0 M_{\odot}$) requires the choice of the IMF only for the higher main sequence. The IMF Salpeter slope is adopted in Table 1 solutions, since flatter or steeper slopes are discarded by comparison with the observed sample.

2. The volume mass densities in Table 2 are strongly influenced by the low-mass main-sequence IMF and almost independent of the different solutions for the SFR in Table 1. The volume density corresponding to the TS IMF case ($\sim 0.07 M_{\odot} \text{ pc}^{-3}$) requires a drastic reduction of the local mass density of the interstellar matter to fill the gap between the dynamical mass determinations and the mass density of the stellar components. From the volume density of Table 2 we deduce the absolute scale of the SFR. The solutions for the TS IMF case, shown in Figure 8, are in agreement with the present-day value of the SFR ($0.01 M_{\odot} \text{ Gyr}^{-1} \text{ pc}^{-3}$). The hypothesis of a Salpeter IMF over the entire mass range seems definitely ruled out.

3. The total surface mass density in $M_{\odot} \text{ pc}^{-2}$ determined according to Hernandez et al. (2000) is significantly different for the two IMF hypotheses. For the TS IMF case (two slopes for the IMF) the present SFR and the total surface mass density of the stellar component are $2 M_{\odot} \text{ Gyr}^{-1} \text{ pc}^{-2}$ and about $45 M_{\odot} \text{ pc}^{-2}$, respectively, values compatible with recent observational estimates.

4. The ratio $R_{\text{He/MS}}$ could constrain the higher main-sequence initial mass function. There is a degeneracy between the SFR and the IMF parameter, x , and different combinations of them can satisfy the conditions requested for reliable MS solutions (§ 7.1). As the ratio $R_{\text{He/MS}}$ has the very important property of being almost independent of the particular shape of the SFR and at the same time *very sensitive* to the parameter x of the IMF, it would be conclusive for the IMF determination. Unfortunately because of the still existing uncertainties on the input physics of the stellar models (related to overshooting and/or mixing, for example) we cannot be confident about its theoretical value, which depends on the ratio between the hydrogen- and helium-burning lifetime of the stellar models. In all the models of Table 1, the ratio $R_{\text{He/MS}}$ is a factor 1.5 greater than the observed one. If one excludes the possibility of some unforeseen selection effects, this means that the evolutionary models are probably inadequate and present values of the theoretical lifetime ratios are greater than the observed values derived from real star distributions in the HRD. As reviewed by Chiosi (1999) and Bertelli (2000), stars

whose turnoff mass is pertinent to the age range under consideration (say from 0.1 to 8–9 Gyr) may be severely affected by the problem of convective overshooting during both core H- and He-burning phases. This topic is far from being settled. Furthermore, it is also complicated by the fact that for stars in the mass range 1 to 1.5–1.6 M_{\odot} during the MS phase the convective core tends first to grow during a sizable fraction of the H-burning lifetime and then to shrink. Whether or not in these circumstances convective overshooting from the H-burning core can grow to full efficiency is still a matter of vivid debate (Aparicio et al. 1990; Rosvick et al. 1998; Chiosi 1999; Bertelli 2000 for a recent review). All this makes stellar models in this mass range still highly uncertain, at least as far as detailed predictions are concerned. For these reasons we have given a different

weight to the results coming from the MS analysis and to those coming from the red region.

We warmly thank Xavier Hernandez for helpful discussions and suggestions, and Peter Stetson for a critical reading of the manuscript. Special thanks are due to Ron Canterna for his invaluable help to make the text more comprehensible. We are indebted to the referee for many useful comments that helped to improve the paper. The *Hipparcos* sample has been selected by making use of CDS facilities (Centre de Données Astronomiques de Strasbourg, France). This study has been financially supported by Ministero dell'Università e della Ricerca Scientifica e Tecnologica (MURST) and by Consiglio Nazionale delle Ricerche (CNR).

REFERENCES

- Aparicio, A., Bertelli, G., Chiosi, C., & Garcia-Pelayo, J. M. 1990, *A&A*, 240, 262
 Aparicio, A., Gallart, C., & Bertelli, G. 1997a, *AJ*, 114, 669
 ———. 1997b, *AJ*, 114, 680
 Bertelli, G. 2000, in *ASP Conf. Ser.* 198, *Stellar Clusters and Associations: Convection, Rotation, and Dynamos*, ed. R. Pallavicini, G. Micela, & S. Sciortino (San Francisco: ASP), 115
 Bertelli, G., Bressan, A., Chiosi, C., Fagotto, F., & Nasi E. 1994, *A&AS*, 106, 275
 Bertelli, G., Bressan, A., Chiosi, C., & Vallenari, A. 1999, *Baltic Astron.*, 8, 271
 Bertelli, G., Mateo, M., Chiosi, C., & Bressan A. 1992, *ApJ*, 388, 400
 Bertelli, G., Nasi, E., Bressan, A., & Chiosi, C. 1997, in *Hipparcos: Venice 97*, ed. B. Battrick, M. A. C. Perryman, P. L. Bernacca, & K. S. O'Flaherty (ESA SP-402) (Noordwijk: ESA), 501
 Bevington, P. R. 1969, in *Data Reductions and Error Analysis for the Physical Sciences* (New York: McGraw-Hill), 84, 314
 Binney, J., Dehnen, W., & Bertelli, G. 2000, *MNRAS*, 316, 658
 Carraro, G., Girardi, L., & Chiosi, C. 1999, *MNRAS*, 309, 430
 Chiappini, C., Matteucci, F., & Gratton, R. G. 1997, *ApJ*, 477, 765
 Chiosi, C. 1999, in *ASP Conf. Ser.*, *Theory and Tests of Convection in Stellar Structure*, ed. A. Gimenez, E. Guinan, & B. Montesinos (San Francisco: ASP), 9
 Crézé, M., Chereul, E., Bienaymé, O., & Pichon, L. 1998, *A&A*, 329, 920
 Duquennoy, A., & Mayor, M. 1991, *A&A*, 248, 485
 Edvardsson, B., Andersen, J., Gustafson, B., Lambert, D. L., Nissen, P. E., & Tomkin, J. 1993, *A&A*, 275, 101
 Englmaier, P., & Gerhard, O. 1999, *MNRAS*, 304, 512
 ESA. 1997, *The Hipparcos and Tycho Catalogues* (ESA SP-1200) (Noordwijk: ESA)
 Flynn, C., & Fuchs, B. 1994, *MNRAS*, 270, 471
 Fuchs, B., Jahreiss, H., & Flynn, C. 1998, *A&A*, 339, 405
 Gallart, C., Aparicio, A., Bertelli, G., & Chiosi, C. 1996, *AJ*, 112, 1950
 Gallart, C., Freedman, W., Aparicio, A., Bertelli, G., & Chiosi, C. 1999, *AJ*, 118, 2245
 Girardi, L. 1999, *MNRAS*, 308, 818
 Güsten, R., & Mezger, P. 1982, *Vistas Astron.*, 26, 159
 Hanson, R. B. 1979, *MNRAS*, 186, 875
 Hernandez, X., Valls-Gabaud, D., & Gilmore, G. 2000, *MNRAS*, 316, 605
 Holmberg, J., & Flynn, C. 2000, *MNRAS*, 313, 209
 Jimenez, R., Flynn, C., & Kotoneva E. 1998, *MNRAS*, 299, 515
 Kroupa, P., Tout, C. A., & Gilmore, G. 1993, *MNRAS*, 262, 545
 Kuijken, K., & Gilmore, G. 1989a, *MNRAS*, 239, 605
 ———. 1989b, *MNRAS*, 239, 651
 ———. 1991, *ApJ*, 367, L9
 Lutz, T. E., & Kelker, D. H. 1973, *PASP*, 85, 573
 Mazeh, T., Goldberg, D., Duquennoy, A., & Mayor M. 1992, *ApJ*, 401, 265
 Mermilliod, J. C., Rosvick, J. M., Duquennoy, A., & Mayor, M. 1992, *A&A*, 265, 513
 Ng, Y. K., & Bertelli, G. 1998, *A&A*, 329, 943
 Patience, J., Ghez, A. M., Reid, I. N., Weinberger, A. J., & Matthews, K. 1998, *AJ*, 115, 1972
 Perryman, M. A. C., et al. 1995, *A&A*, 304, 69
 ———. 1998, *A&A*, 331, 81
 Pham, H. A. 1997, in *Hipparcos: Venice 97*, ed. B. Battrick, M. A. C. Perryman, P. L. Bernacca, & K. S. O'Flaherty (ESA sp-402) (Noordwijk: ESA), 559
 Pont, F., Mayor, M., Turon, C., & VandenBerg, D. A. 1998, *A&A*, 329, 87
 Preibisch, T., Balega, Y., Hofmann, K.-H., Weigelt, G., & Zinnecker, H. 1999, *NewA*, 4, 531
 Press, W. H., Teukolsky, S. A., Vetterling, W. T., & Flannery, B. P. 1986, in *Numerical Recipes in Fortran* (Cambridge: Cambridge Univ. Press), 617
 Reid, I. N. 1997, *AJ*, 114, 161
 Rocha-Pinto, H. J., & Maciel, W. J. 1996, *MNRAS*, 279, 447
 ———. 1997, *MNRAS*, 289, 882
 Rocha-Pinto, H. J., Scalo, J., Maciel, W. J., & Flynn, C. 2000, *ApJ*, 531, L115
 Rosvick, J. M., & VandenBerg, D. A. 1998, *AJ*, 115, 1516
 Schröder, K. P. 1998, *A&A*, 334, 901
 Trimble, V. 1990, *MNRAS*, 242, 79
 Turon, C., et al. 1992, *A&A*, 258, 74
 Vallenari, A., Chiosi, C., Bertelli, G., Aparicio, A., & Ortolani, S. 1996a, *A&A*, 309, 367
 Vallenari, A., Chiosi, C., Bertelli, G., & Ortolani, S. 1996b, *A&A*, 309, 358